Mouse model of experimental pulmonary hypertension: Lung angiogram and right heart catheterization

Mingmei Xiong[1,2]*, Pritesh P. Jain[1,]*, Jiyuan Chen[1,3], Aleksandra Babicheva[1], Tengteng Zhao[1], Mona Alotaibi[4], Nick H. Kim[4], Ning Lai[1,3], Amin Izadi[1], Marisela Rodriguez[1], Jifeng Li[1,5] ⬩, Angela Balistrieri[1], Francesca Balistrieri[1], Sophia Parmisano[1], Xin Sun[6], Daniela Voldez-Jasso[7], John Y.-J. Shyy[8], Patricia A. Thistlethwaite[9], Jian Wang[1,3], Ayako Makino[10] ⬩ and Jason X.-J. Yuan[1] ⬩

[1]Section of Physiology, University of California, San Diego, La Jolla, CA, USA; [2]Department of Critical Care Medicine, Guangzhou Medical University, The Third Affiliated Hospital of Guangzhou Medical University, Guangzhou, China; [3]State Key Laboratory of Respiratory Disease, Guangzhou Medical University, Guangzhou, China; [4]Division of Pulmonary, Critical Care and Sleep Medicine, University of California, San Diego, La Jolla, CA, USA; [5]Beijing Chaoyang Hospital, Capital Medical University, Beijing, China; [6]Department of Pediatrics, University of California, San Diego, La Jolla, CA, USA; [7]Department of Bioengineering, University of California, San Diego, La Jolla, CA, USA; [8]Division of Cardiovascular Medicine, Department of Medicine, University of California, San Diego, La Jolla, CA, USA; [9]Department of Surgery, University of California, San Diego, La Jolla, CA, USA; [10]Division of Endocrinology and Metabolism, University of California, San Diego, La Jolla, CA, USA

Abstract

Pulmonary arterial hypertension is a progressive and fatal disease and rodents with experimental pulmonary hypertension (PH) are often used to study pathogenic mechanisms, identify therapeutic targets, and develop novel drugs for treatment. Here we describe a hands-on set of experimental approaches including ex vivo lung angiography and histology and in vivo right heart catheterization (RHC) to phenotypically characterize pulmonary hemodynamics and lung vascular structure in normal mice and mice with experimental PH. We utilized Microfil polymer as contrast in our ex vivo lung angiogram to quantitatively examine pulmonary vascular remodeling in mice with experimental PH, and lung histology to estimate pulmonary artery wall thickness. The peripheral lung vascular images were selected to determine the total length of lung vascular branches, the number of branches and the number of junctions in a given area (mm^{-2}). We found that the three parameters determined by angiogram were not significantly different among the apical, middle, and basal regions of the mouse lung from normal mice, and were not influenced by gender (no significant difference between female and male mice). We conducted RHC in mice to measure right ventricular systolic pressure, a surrogate measure for pulmonary artery systolic pressure and right ventricle (RV) contractility ($RV \pm dP/dt_{max}$) to estimate RV function. RHC, a short time (4–6 min) procedure, did not alter the lung angiography measurements. In summary, utilizing ex vivo angiogram to determine peripheral vascular structure and density in the mouse lung and utilizing in vivo RHC to measure pulmonary hemodynamics are reliable readouts to phenotype normal mice and mice with experimental PH. Lung angiogram and RHC are also reliable approaches to examine pharmacological effects of new drugs on pulmonary vascular remodeling and hemodynamics.

Introduction

Pulmonary hypertension (PH) is a complex disorder that is classified into five major forms based on etiological causes, pathological characteristics, clinical manifestation, and therapeutic interventions.[1–5] It is estimated that PH affects

*These authors contributed equally to this work.

Corresponding author:
Jason X.-J. Yuan, Section of Physiology, Division of Pulmonary, Critical Care and Sleep Medicine, University of California, San Diego, 9100 Gilman Drive (MC 0856), La Jolla, CA 92093-0856, USA.
Email: jxyuan@health.ucsd.edu

over 100 million people worldwide.[6] Regardless of the initial pathogenesis, increased pulmonary vascular resistance (PVR) and elevated pulmonary arterial pressure (PAP) reinforce hemodynamic burden onto the right ventricle (RV), ultimately causing RV dysfunction and right heart failure. Despite significant advances in our understanding of the pathogenic mechanisms of PH and clinical improvements in patient care, outcomes for severe PH like pulmonary arterial hypertension (PAH) are still poor and treatments are limited. In vitro and histological/pathological studies on patient lung specimens are mainly restricted to the end-stage of PH; it is also difficult to study structural and functional alterations of the pulmonary vasculature during the disease progression and to test pharmacological effect of newly synthesized chemicals on normal subjects and patients. The multifactorial nature of the disease, PAH or other forms of severe PH, involves complex underlying mechanisms that are difficult to study in patients. Simplified in vitro systems (tissues and cells isolated from patients) and genetic studies have been used to define the cellular and molecular mechanisms of PH or PAH, though the relevance of these studies to patients is not always clear. Therefore, animal models of PH are necessary to apply and validate what has been learned at the laboratory bench in complex living systems. Since the effects of genetic alterations and the efficacy of novel therapies can be tested in the in vivo animal models, the animal models of PH can be used to improve our current treatment for this disease, providing an essential link between the bench and bedside. To further study pathogenic mechanisms and therapeutic interventions of PH, it is therefore important to have a well-characterized mouse model of PH that recapitulates some of the pathophysiological and pathological changes in patients. The mouse model of PH also allows us to define the role of specific genes in the development and progression of experimental PH using global, conditional, and inducible knockout as well as transgenic mice.[7–12]

Stenmark et al.[13] elegantly and extensively described the various animal models widely used in studying pathogenic mechanisms and therapeutic interventions on PH. Animals with chronic hypoxia-induced PH are commonly used in vivo model to study pathogenic mechanisms and therapeutic interventions due to the model's predictability and reproducibility. Nevertheless, responses to chronic hypoxia vary among different animal species. The most commonly used animal species are mice and rats.[14] Chronically hypoxic mice exhibit significant increases in pulmonary artery (PA) pressure with minimal vascular remodeling compared to rats.[15–17] The most common observations are muscularization of non-muscularized vessels and minimal wall thickening of muscular resistance arteries.[17] Chronic hypoxia-induced PH models do not exhibit plexiform lesions as seen in 15–20% of patients with idiopathic PAH.[18–21] Thus, the chronic hypoxia-induced PH models should be regarded as a model with mild PH. The most common model for severe PH is Sugen/hypoxia-induced PH model where Sugen 5416 (Su 5416), an inhibitor of the VEGF receptor is injected subcutaneously before (for rats) and during (for rats and mice) exposure to hypoxia. VEGF is a critical factor for vascular endothelial cells. Upon its inhibition, a severe PH with abnormal endothelial proliferation was observed in Sugen/Hypoxia-induced PH model. Furthermore, Sugen in combination with chronic hypoxia further enhance pulmonary vascular cell proliferation and vascular wall thickening. The Sugen/Hypoxia-induced PH model is a persistent model exhibiting severe PH even upon returning to normoxia in rats.[22]

In this study, we sought to characterize a commonly used mouse model of mild and severe PH in the ex vivo angiography and in vivo pharmacological experiments on pulmonary vascular remodeling, pulmonary hemodynamics, and right heart function with a detailed hands-on protocol and experimental approach. The study provides strong evidence that the mouse model of PH is a simple, systematic, and reliable model for ex vivo and in vivo pharmacological experiments used to examine the prevention, or inhibitory, and regression, or therapeutic, effects of various drugs administered orally or intraperitoneally on experimental PH. The results obtained from animal models of PH will help guide clinical research on patients with PH and PAH in developing novel and effective therapies.

Methods

Experimental animals

Adult male and female C57BL/6 mice (7–8 weeks and ~25 g body weight) were used for ex vivo experiments to examine lung angiogram to determine pulmonary vascular remodeling and in vivo (using intact animal to assess hemodynamic changes) experiments. All animal care and experimental protocols were approved by the Institutional Animal Care and Use Committee (IACUC) of the University of California, San Diego (La Jolla, CA) and executed according to the IACUC guidelines complying with national and international regulations. All animals were housed in cages provided by the accredited animal facilities with 12-h light and dark cycles. Mice food and tap water were provided as libitum.

To establish chronic hypoxia-induced PH (HPH), a mild PH model, mice were placed in normobaric hypoxic chambers (Cat. #A30271-P, BioSpherix, Lacona, NY) equilibrated with hypoxic gas mixture (10% O_2 in N_2) for four weeks. The hypoxic chamber contained an O_2 sensor (Cat. # ProOx P110-E702) continuously monitoring O_2 concentration and PO_2 inside of the chamber to adjust the flow of flushed 10% O_2. The normoxic control mice were placed in the same animal room in which the mice were exposed to 21% O_2 (in N_2). The feed, bedding, and water for mice were changed once a week. The numbers of mice used for the experiments

are detailed in the figure legend. In general, five or more mice were used per group for each study.

To establish Sugen/Hypoxia-induced PH (SuHx-PH), a severe PH model, based on the protocol used to induce SuHx-PH in rats.[22] Sugen5416 (SU5416) is a VEGF receptor inhibitor that has been shown to cause severe PH in mice.[23] The protocol for inducing SuHx-PH in mice was similar to that for rats with more subcutaneous injections of SU5416 during hypoxic exposure. The dose of SU5416 used in this study was 20 mg/kg body weight,[22] which was injected once a week during the six-week exposure to hypoxia. This is quite different from the protocol for rats in which only one dose of SU5416 was given at the first day of hypoxic exposure[24–26]; it has been demonstrated that mice are less susceptible to SU5416.

In vivo pharmacological experiments

In this study, the prevention experimental protocol was used to examine the effect of 2-aminoethyl diphenylborinate (2-APB, D9754, Sigma, St. Louis, MO), a blocker of non-selective cation channels including TRP channels[27–32] in mice with chronic hypoxia-induced PH (HPH). 2-APB was intraperitoneally (i.p.) administered once a day (q.d.) at the beginning of hypoxic exposure and for the entire duration of hypoxic exposure (four weeks). The prevention experimental protocol was designed to test whether the drug prevents (or attenuates) the animals from developing experimental PH or HPH in this case. For the prevention experiments using 2-APB, mice were randomly divided into three groups (n = 5 mice per group): (i) Normoxia+vehicle (DMSO) group (Nor+Veh), (ii) Hypoxia+vehicle group (Hyp+Veh), and (iii) Hypoxia+2-APB group (Hyp+2-APB). In the Hyp+Veh and Hyp+2-APB groups, DMSO and 2-APB (1 mg/kg body weight) were intraperitoneally (i.p.) injected, respectively, into mice at the same time each day for four weeks.

Following hypoxic exposure and drug treatment, mice were anesthetized by continuous inhalation of isoflurane (1.5%) and then right heart catheterization (RHC) was conducted to measure right ventricle pressure (RVP) and right ventricle (RV) contractility (RV $\pm$ dP/dt) using a mouse Pressure volume (PV) catheter (Millar Instruments, PVR1030, Houston, TX, USA) inserted into the RV via the external right jugular vein. Baseline calibration was performed for the catheter before each measurement to ensure that the basal pressure was zero. RVP and RV $\pm$ dP/dt were recorded and analyzed using the AD Instruments Lab Chart software. The mean pulmonary arterial pressure (mPAP) was estimated based on the right ventricular systolic pressure (RVSP) using the equation: mPAP (in mmHg) = $0.61 \times RVSP + 2$.[33,34] The RV contractile index was calculated as the ratio of RV $\pm$ dP/dt$_{max}$ to RVSP, a surrogate measure of pulmonary arterial systolic pressure.

Lung angiogram

Male and female C57Bl/6 mice were first anesthetized using sodium pentobarbital (Euthasol®, Virbac, 200-071) (120 mg/kg, i.p.). To prevent blood coagulation or pulmonary embolism, heparin (20 IU) was immediately injected in to the RV when chest wall was opened and the anterior wall was removed. A PE-20 tube was then inserted into the main PA through the RV and warm PBS (pH=7.4 at 36–38°C) was superfused through the tube at a speed of 0.05 ml/min for 3 min to flush out residual blood in the pulmonary vasculature. Freshly prepared Microfil® polymer mixture (MV-122, Flow-Tech Inc., Carver, MA), as contrast dye for angiogram, was then gently instilled into the PA perfusate via a syringe pump (Farmingdale, NY, USA) at the same speed for 1–2 min until the Microfil® polymer mixture reached the peripheral branches of pulmonary artery. Then, the Microfil®-filled lungs and heart were isolated and soaked in PBS overnight at 4°C. Twenty-four hours later, the Microfil®-filled lungs were dehydrated in ethanol by immersing the lungs into 50%, 70%, 80%, 95%, and 100% ethanol solutions, respectively. The dehydrated lungs were then put into a methyl salicylate (Sigma-Aldrich) solution and then placed on a shaker overnight. When the lungs became translucent and the Microfil® polymer was clearly visible, the lungs were photographed with a digital camera (MU1000, FMA050, Amscope, CA, USA) through a dissecting microscope (WILD M651, Leica, Switzerland). The lung peripheral vascular branch images (1 mm from the edge of the lung) were selected using Adobe Photoshop software and quantified by ImageJ to calculate the total length of vascular branches, the number of branches, and the number of branch junctions in the pulmonary vascular networks.

RV hypertrophy measurement

RV hypertrophy was measured by calculating the ratio of the weight of the RV to the weight of the left ventricle (LV) and the septum (S) [RV/(LV+S)]. The weight or the RV, LV, and S should be measured right after pulmonary hemodynamic measurement. Briefly, right after measurement of RVP, the whole heart was isolated and dissected from the animal. After removal of the atrium, the ventricular chambers were gently aspirated or washed with saline to remove blood. Using the main pulmonary artery for anatomic orientation, we then carefully isolated the RV from the atria-free heart. The RV and the remaining heart tissue (LV+S) were weighed using an analytic balance with a sensitivity of 0.0001 g, and the RV/(LV+S) ratio, also referred to as the Fulton Index, was then calculated accordingly.

Lung arterial wall thickness measurement

The Aperio ImageScope system was used to measure PA wall thickness. Briefly, mouse lungs were isolated and perfused with cold PBS solution to remove blood and then

fixed in a 10% normalized formalin solution overnight. The fixed lung tissues were dehydrated and further processed for hematoxylin and eosin (H&E) staining. The H&E-stained lung tissue slides were scanned with the Aperio scanner. Using the Aperio ImageScope software (version 11), the largest external and internal diameters as well as external and internal areas for each PA were measured. The PA wall thickness was calculated as (external vessel area – internal vessel area)/(external vessel area), as described previously.[35] The diameter was measured for each PA and the PA was categorized into three groups based on the external diameter (ø): small PA with ø $< 50\,\mu m$, middle-sized PA with ø $= 50$–$100\,\mu M$, and large PA with ø $>100\,\mu m$. Moreover, 5–10 PA were used of each size per mouse for data analysis.

Statistical analysis

Statistical analysis of experimental data were conducted using SigmaPlot 11.0 and ImageJ softwares. Summarized data are expressed as mean $\pm$ standard error (SE). Statistical analysis was performed using paired or unpaired Student's t-test (for two groups) or one-way ANOVA (for multiple groups). Differences were considered statistically significant at $p < 0.05$. A significant difference is expressed in the figures or figure legends by $*p < 0.05$, $**p < 0.01$, and $***p < 0.001$.

Results

In this study, we aimed to provide a hands-on experimental approach on mouse models of PH to study pulmonary vascular remodeling and test drug effects on established pulmonary vascular abnormalities in mice with experimental PH. We used (*i*) ex vivo lung angiogram and lung histology to study changes of pulmonary vascular structure and pulmonary vascular remodeling, and (*ii*) in vivo pulmonary hemodynamic measurement to conduct pharmacological experiments to confirm the experimental model of PH in mice and study drug effect on the development and progression of experimental PH.

Ex vivo lung angiogram

Lung angiography is used to visualize the pulmonary vasculature from the main PA to the peripheral PA branches. A continuous ex vivo Microfil® polymer perfusion technique that distends lung vessels evenly in different branches and results in reproducible assessments of lung vascular structure is used to evaluate pulmonary vascular tree in control mice and mice with experimental PH.

Using the ex vivo lung angiography and Microfil® polymer perfusion technique, we first investigated and compared lung peripheral vascular branches in different regions, such as the apical (Api), middle (Mid), and basal (Bas) regions, of the mouse lungs. The step-by-step protocol for

conducting ex vivo angiography is described in the Box 1 and in the schematic diagram (Fig. 1).

Using the experimental protocol shown above and in Fig. 1, we compared the total length of lung vascular branches, the number of branches, and the number of junctions in different areas of the left lungs. We chose three areas for the comparison from the left lung of mice: (*a*) top lung peripheral area or the apical (Api) area, (*b*) middle lung peripheral area or the middle (Mid) area, and (*c*) bottom lung peripheral area or the basal (Bas) area (Fig. 2a, left panel). In each of the selected Api, Mid, and Bas areas, we further split the peripheral areas to region-A (the most peripheral area) and region-B (the area immediately proximal to the most peripheral area, region-A) (Fig. 2a, middle and right panels). Regions A and B are images obtained at 1 mm edge from the most peripheral area and the area adjacent to the most peripheral area, respectively. The quantitative data showed that the total length of branches, the number of branches, and the number of junctions in selected Api, Mid, and Bas peripheral areas (region-A and region-B) were very close to each other (Fig. 2b). Furthermore, there was no significant difference between region-A and region-B in each of the Api, Mid, and Bas areas (Fig. 2c) or in the sum of all the Api, Mid, and Bas areas (Fig. 2d). These experiments were designed to show how apical, middle, and basal areas (A and B regions) are defined for experimental data analysis and whether angiography parameters (total length of branch, number of branch, and number of junction) at given area are similar among apical, middle, and basal peripheral areas in male and female mice. These data indicate that, for quantifying ex vivo lung angiogram, we should use the peripheral areas of the lung in the apical, middle, or basal area.

The next set of experiments was designed to compare the lung angiography parameters between male and female mice. We chose the same three areas as described above, the apical (Api), middle (Mid), and basal (Bas) peripheral areas of the left lungs (Fig. 3a and b). The total length of lung vascular branches, the number of vascular branches, and the number of vascular branch junctions in the Api, Mid, and Bas peripheral areas (region-A and region-B) in lungs from male mice were indifferent from those in lungs from female mice (Fig. 3c). In addition, the angiography parameters were all comparable between male and female mice in region-A and region-B in each of the Api, Mid, and Bas areas (Fig. 3d) or in the total APi, Mid, and Bas areas (Fig. 3e). When we analyzed the angiography parameters in the whole lungs, we also did not observe any differences between male and female mice (Fig. 3f and g). These data indicate that the total length of branches, the number of branches, and the number of junctions revealed by ex vivo lung angiography in selected apical, middle, and basal areas or in the whole lungs are similar between male and female mice.

Box 1 Protocol for ex vivo angiography using mouse lungs.

1. Anesthetize mouse with intraperitoneal (i.p.) injection of pentobarbital (120 mg/kg body weight). Make sure that the mouse is deeply anesthetized (i.e., no reflex response while pinching lower limbs).
2. Restrain mouse on surgical pad under microscope with ventral side facing up.
3. Make a 2- to 3-cm horizontal incision in the abdomen just below the diaphragm, cut ribs vertically through the diaphragm to open the chest and expose the heart and lungs.
4. Heparin was injected in the right ventricle to prevent blood coagulation.
5. Remove the adipose tissue and thymus around the heart and large vessels (aorta and main PA).
6. Prepare a catheter using PE-20 tubing of 10-cm length attached with 25G needle.
7. Make a small incision at the base of the main PA and insert the catheter into PA via the right ventricle and perfuse warm PBS at a speed of 0.05 ml/min for 3 min using an automated syringe pump (Micro-Harvard) until lung turns completely white.
8. Freshly prepare the Microfil polymer casting solution and infuse 0.08 ml of Microfil into the lung via the RV and PA until lung appears yellow. Make sure that Microfil polymer mixture has no air bubbles.
9. Cover the Microfil polymer-filled lungs (and heart) with saline-soaked paper towel to avoid desiccation and let it set overnight at 4°C.
10. Next day, after Microfil is polymerized, isolate the heart and lungs, place them in 15 ml polypropylene centrifuge tube filled with PBS, and place the tubes on a gentle shaker at room temperature for 15 min.
11. Replace PBS in the tubes with 50% ethanol and gently shake the tube for 1 h at room temperature. Replace 50% ethanol with 70% ethanol and gently shake the tube for 1 h; repeat this step for 80%, 95%, and 100% (2 times for 100% ethanol), respectively, to completely dehydrate the lung tissue.
12. Replace 100% ethanol in the tube with methyl salicylate (under a fume hood) and gently shake the tube overnight at RT until the lung tissue becomes translucent with Microfil clearly visible.
13. Take photograph of the lungs with a microscope camera at 8× and 30× magnification.
14. Use Adobe Photoshop software to manually outline the lung peripheral region (1 mm width from the edge of the lung) for vascular density analysis.
15. Use NIH Image J software to convert the manually outlined image to the binary image, and calculate the total length of vascular branches, the number of vascular branches and the number of junctions in the skeletonized images. Data were normalized by the area selected within the edge of peripheral vascular lung.

In order to increase experimental efficiency and limit the number of animals used in the in vivo experiments, we conducted lung angiography experiments after RHC in certain animals. Using the same protocol described above, we compared the angiography parameters between control mice without RHC (–RHC) and the mice right after RHC (+RHC). The data obtained from the Api, Mid, and Bas peripheral areas of the left lungs (Fig. 4a and b) from –RHC and +RHC mice showed that the total length of lung vascular branches, the number of vascular branches, and the number of vascular branch junctions were not different in region-A and region-B from the Api, Mid, and Bas areas (Fig. 4c). Similarly, we did not observe significant difference of the angiography parameters in region-A and region-B in each of the Api, Mid, and Bas areas (Fig. 3d) or in the total APi, Mid, and Bas areas (Fig. 4e) between –RHC and +RHC mice. Again, when we analyzed the angiography parameters in the whole lungs, we did not observe any difference of the angiography parameters between –RHC and +RHC mice (Fig. 4f and g). These data indicate that a short-time procedure (4–6 min) of RHC in mice does not significantly affect the ex vivo angiography parameters.

Lung histology

Pulmonary vascular remodeling including concentric PA wall thickening and occlusive intimal lesions is one of the major causes for the elevated PVR and PAP in patients with idiopathic PAH and animals with mild and severe experimental PH. In addition to the ex vivo lung angiogram, we also used lung histology to visualize and quantify PA wall thickness in mouse lungs. To examine PA wall thickening in mice, the lung was dissected en-block and perfused with 10% formalin through the trachea, and the fixed lung was then sliced and stained with hematoxylin and eosin (H&E). The PA wall thickness was then measured by the protocol shown in the Box 2 and in Fig. 5a.

Using this protocol (Fig. 5a), we examined and compared the PA wall thickness of large PAs (OD $> 100\,\mu m$) (Fig. 5b), medium-sized PAs (OD $= 50$–$100\,\mu m$) (Fig. 5c), and small PAs (OD $< 50\,\mu m$) (Fig. 5d) in the lungs from normoxic control mice and chronically hypoxic mice (Fig. 5e and f). In the cross-section original image of PA (Fig. 5a), we first constructed an image showing the total PA area (A_T) including the PA wall and intraluminal area, and then we removed the PA intraluminal area (A_{in}) to show or measure the PA-wall area (A_{PA}). PA wall thickness was defined in this study as the ratio of the PA-wall area (A_{PA}) to the total area (A_T): PA wall thickness $= A_{PA}/A_T = A_{PA}/(A_{PA}\text{-}A_{in})$. Contribution of PA wall thickening to pulmonary vascular resistance varies in the large, middle-sized, and small PA or depends on the intraluminal diameter of the PA. The shape of PA in the cross-section image is often irregular, which makes it
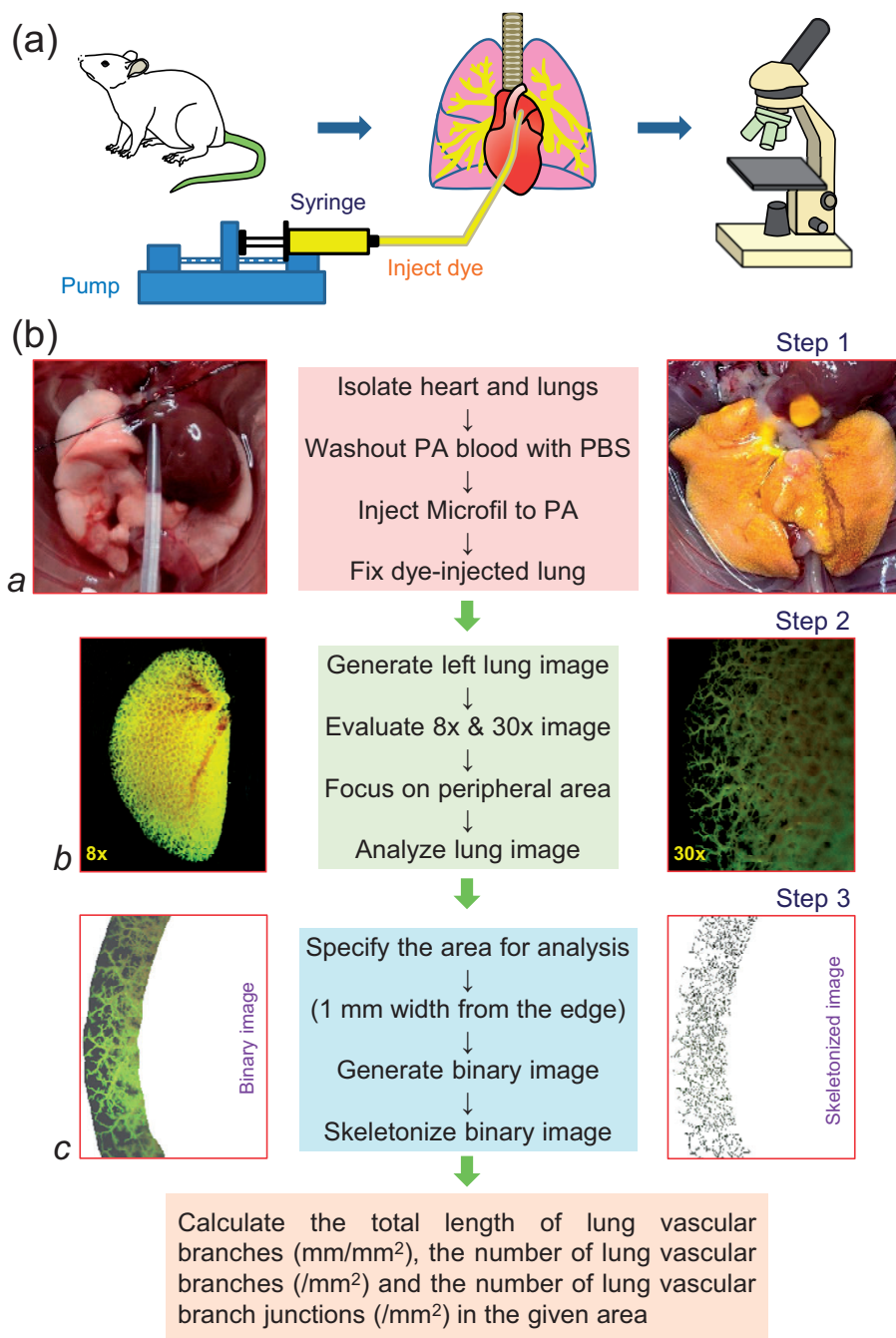
Fig. 1. Schematic diagram showing the experimental protocol and approach for mouse lung angiography. (a) The main equipment used in the procedure including the animal (mouse) and isolated lungs, an automatic syringe pump and the dissecting microscope with a digital camera. (b) The protocol for preparing the lungs for infusing contrast, imaging lung vessels and quantifying vascular branches. A polyethylene tube is cannulated into the main PA via the RV in an anesthetized mouse to superfuse Microfil® polymer (yellow) into the lung vasculature using the automated pump (a). The lungs filled with Microfil are then dehydrated in ethanol and placed in methyl salicylate for overnight to show only the vasculature (b). The left lung image is generated with a digital camera through a dissecting microscope (b). The whole lung is first photographed at 8× magnification (b, left panel), then different regions (the apical, middle, or basal region) of the left lung were photographed at 30× magnification (b, right panel). The peripheral lung vascular images from the upper (apical), middle, and low (basal) regions were selected and converted to binary images for quantitative analysis using ImageJ software (c).

difficult to calculate or measure the intraluminal diameter of the PA. We therefore used the PA intraluminal area (A_{in}) to normalize PA wall thickness or the ratio of the PA-wall area (A_{PA}) to the total area (A_T) [(A_{PA}/($A_{PA} - A_{in}$)] to indicate PA wall thickness. As shown i Fig. 5, chronic exposure to hypoxia for four weeks
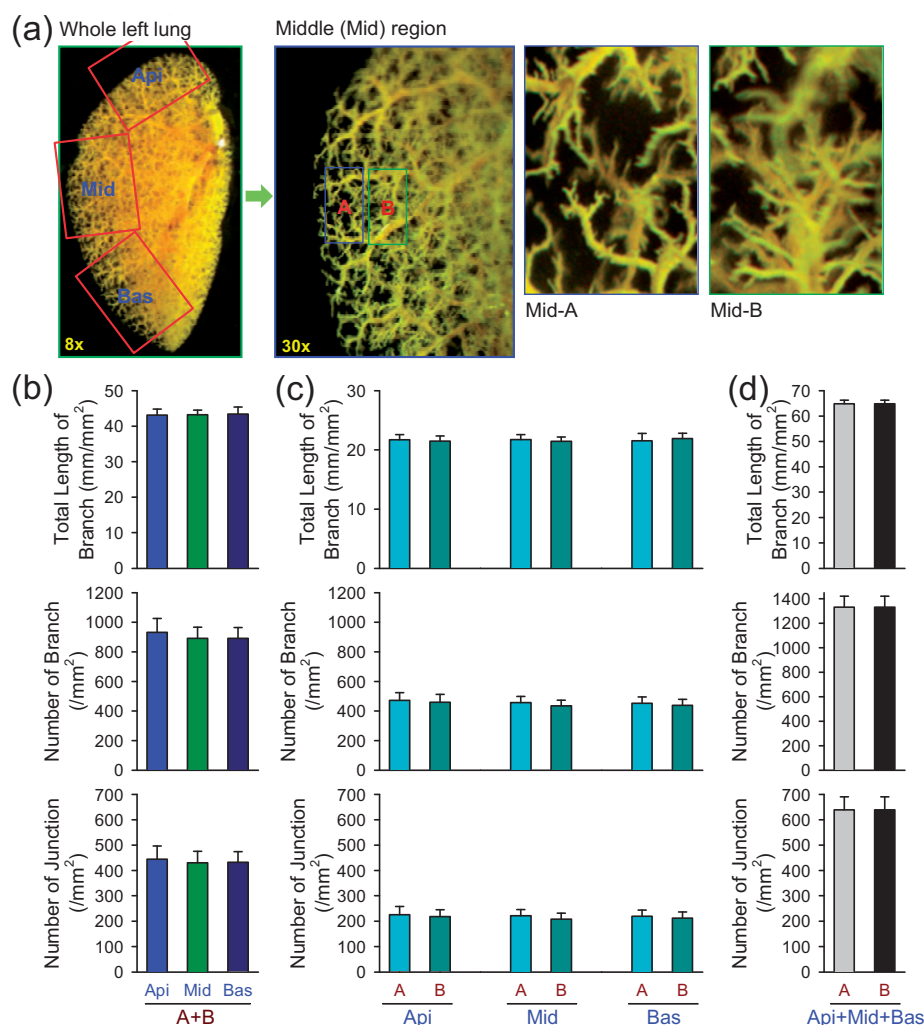
Fig. 2. Comparison of angiography parameters in different peripheral regions of mouse lung. (a) Representative angiograph images of the whole left lung at 8× magnification and the middle (Mid) peripheral region of the left lung at 30× magnification (left panels). Enlarged angiograph images of the labeled middle (Mid) region (30×) depicting the most peripheral region (Mid-A) and the adjacent region (Mid-B). (b–d) Summarized data (mean±SE, n=6) showing the total length of lung vascular branches (upper panels), the number of lung vascular branches (middle panels) and the number of lung vascular branch junctions (lower panels) per square millimeter from the selected apical (Api), middle (Mid), and basal (Bas) lung areas (b), the selected most peripheral areas (A) and adjacent peripheral areas (B) in the Api, Mid, and Bas lung regions (c), and the combined (A+B) peripheral areas in the Api, Mid and Bas lung regions (d) from normal female and male mice.

significant increased PA wall thickness in large PAs (OD > 100 μm) (by 82.5 ± 9.6%, n = 15; Fig. 5b), medium-sized PAs (OD = 50–100 μm) (by 83.5 ± 8.5%, n = 15; Fig. 5c), and small PAs (OD < 50 μm) (by 87.9 ± 6.5%, n = 15; Fig. 5d) in comparison to normoxic control mice.

Lung hemodynamics

RHC was conducted in mice to measure pulmonary hemo-dynamics. The Millar catheter we used for RHC in mice had a straight catheter tip, so we were unable to place the cath-eter into the PA to directly measure pulmonary arterial pressure (PAP). We were able to measure right ventricular pressure (RVP), so we used RVSP as a surrogate measure

for pulmonary artery systolic pressure (PASP), and estimat-ed mean PAP based on the equation: $mPAP = 0.61 \times RVSP + 2$ (in mmHg)[33] (Fig. 6a and b). When the catheter was placed in the RV, we were also able to measure RV contractility (RV ± dP/dt) and then calculated the RV contractile index $[= (RV \pm dP/dt_{max})/RVSP]$.[36,37] The RVP and RV ± dP/dt were measured by the protocol shown in the Box 3 and in Fig. 6a and b.

Among more than 100 normal mice for which we con-ducted RHC, the averaged values of RVSP (ranging from 16 to 26 mmHg; Fig. 6c), RV ± dP/dt$_{max}$ (ranging from 1000 to 4000 mmHg/s; Fig. 6d), and heart rate (HR, ranging from 250 to 650 beats per min) are 21 mmHg, 1855 mmHg/s, and 471 bpm, respectively. As shown in the histograms of RVSP, RV ± dP/dt$_{max}$, and HR from the measurement of
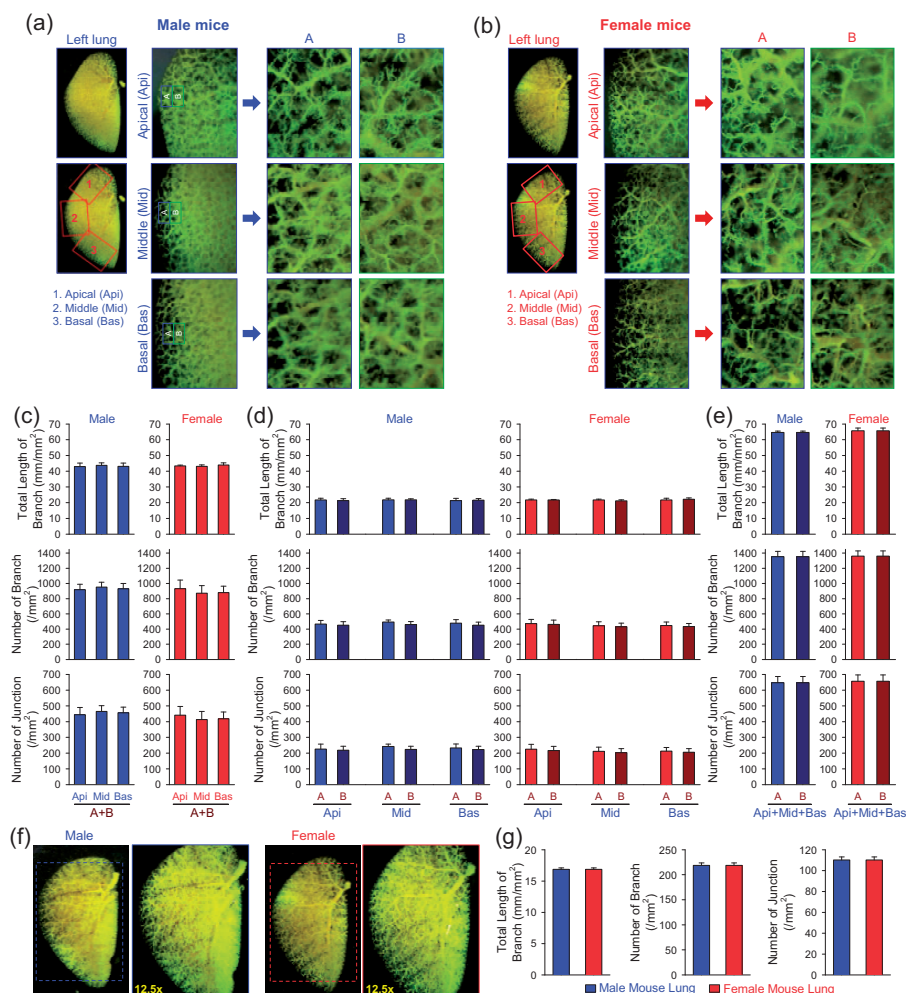
Fig. 3. Comparison of angiography parameters in different peripheral regions of the lung between male and female mice. (a and b) Representative angiograph images of the whole left lung at 8× magnification and the peripheral regions of the apical (Api, 1), middle (Mid, 2), and basal (Bas, 3) areas of the left lung at 30× magnification (left panels) from male (a) and female (b) mice. Enlarged angiograph images of the labeled Api, Mid and Bas areas (30×) depicting the most peripheral region (A) and the adjacent region (B) from male (a) and female (b) mice. (c and e) Summarized data (mean ± SE, n = 9) showing the total length of lung vascular branches (upper panels), the number of lung vascular branches (middle panels) and the number of lung vascular branch junctions (lower panels) per square millimeter from the selected Api, Mid and Bas lung areas (c), the selected most peripheral areas (A) and adjacent peripheral areas (B) in the Api, Mid and Bas lung regions (d), and the combined (A+B) peripheral areas in the Api, Mid and Bas lung regions (e) from normal male (blue) and female (red) mice. (f) Representative angiograph images showing the whole left lung at 8× and 12.5× magnification from male (left panels) and female (right panels) mice. (g) Summarized data (mean ± SE, n = 9) showing the total length of lung vascular branches (left panel), the number of lung vascular branches (center panel) and the number of lung vascular branch junctions (right panel) per square millimeter of the whole-lung images from normal male (blue) and female (red) mice.

106–130 mice, the measured values for all three parameters seems to be normal distribution (Fig. 6c–e) in normal mice.

Many animal models have been established to study pulmonary vascular diseases. Stenmark et al. elegantly evaluated many of the animal models of PH in an extensive review article.[13] Here we briefly describe two commonly used mouse models of PH: mice with chronic hypoxia-induced PH (HPH, a mouse model for mild PH) and mice with Sugen-hypoxia-induced PH (SuHx-PH, a mouse model for severe PH), based on the hemodynamic measurements using RHC. For HPH model, the mice were placed in a normobaric hypoxic chamber equilibrated with 10% O_2 in

N_2 and maintained under hypoxic conditions for four weeks before lung hemodynamics were measured. The normoxic control mice were housed in the same animal room under room air (21% O_2). We used a slightly modified procedure to establish SuHx-PH mouse model: mice were injected with Sugen5416 (20 mg per kg body weight) at the beginning of exposure to hypoxia followed by injection once a week during the four-week normobaric hypoxia exposure.

As shown in Fig. 6f and g, we compared the hemodynamics in normoxic control mice (Nor), HPH mice (Hyp), and mice with SuHx-PH (Sug+Hyp) (Fig. 6f and g). RVSP was significantly increased from 20.8 ± 05 mmHg in Nor
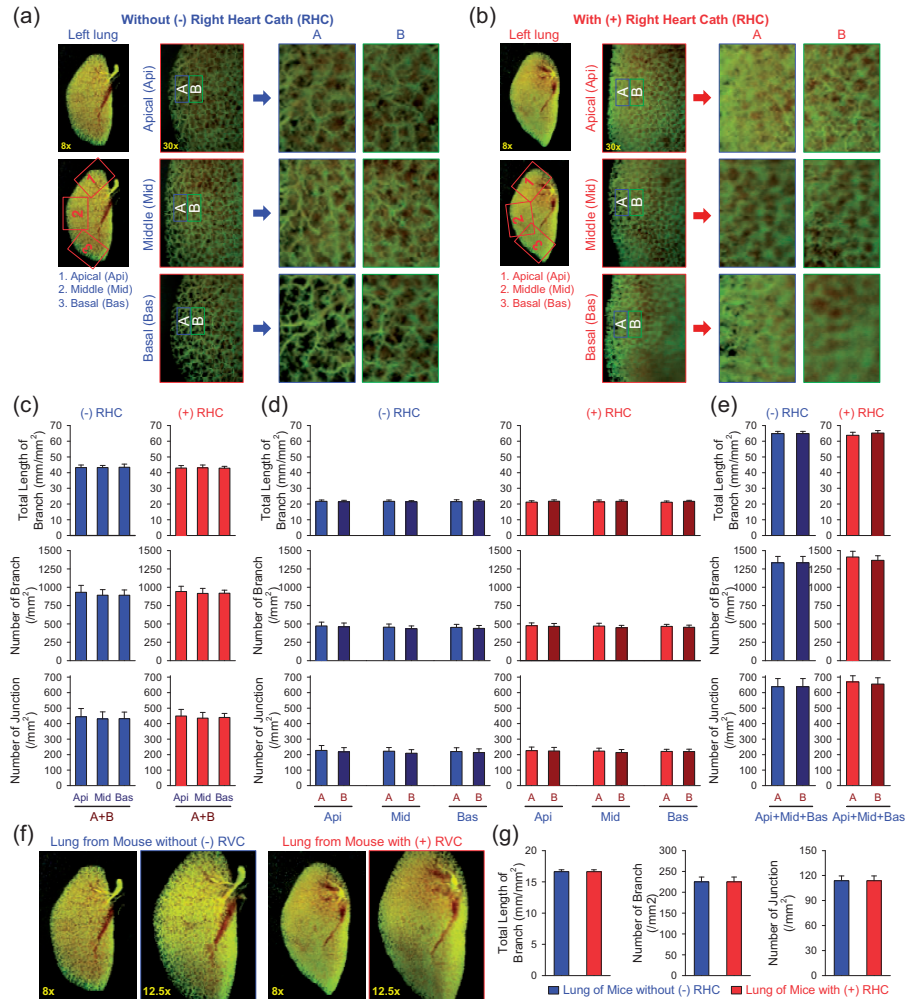
Fig. 4. Effect of right heart catheterization on angiography parameters in the peripheral regions of the mouse lungs. (a and b) Representative angiograph images of the whole left lung at $8\times$ magnification and the peripheral regions of the apical (Api, 1), middle (Mid, 2) and basal (Bas, 3) areas of the left lung at $30\times$ magnification (left panels) from mice without (-, a) or with ($+$, b) right heart catheterization (RH Cath or RHC). Enlarged angiograph images of the labeled Api, Mid and Bas areas ($30\times$) depicting the most peripheral region (A) and the adjacent region (B) from mice without (–RHC, a) or with ($+$RHC, b) right heart cath. (c and e) Summarized data (mean$\pm$SE, n$=$16) showing the total length of lung vascular branches (upper panels), the number of lung vascular branches (middle panels) and the number of lung vascular branch junctions (lower panels) per square millimeter from the selected Api, Mid and Bas lung areas (c), the selected most peripheral areas (A) and adjacent peripheral areas (B) in the Api, Mid and Bas lung regions (d), and the combined (A$+$B) peripheral areas in the Api, Mid and Bas lung regions (e) from –RHC mice (blue) and $+$RHC mice (red). (f) Representative angiograph images showing the whole left lung at $8\times$ and $12.5\times$ magnification from –RHC and $+$RHC mice. (g) Summarized data (mean$\pm$SE, n$=$16) showing the total length of lung vascular branches (left panel), the number of lung vascular branches (center panel) and the number of lung vascular branch junctions (right panel) per square millimeter of the whole-lung images from –RHC mice (blue) and $+$RHC mice (red). The –RHC and $+$RHC mice include both male and female mice.

mice to 31.4 ± 0.87 mmHg in Hyp mice ($p<0.001$) and 38.9 ± 0.8 mmHg in Sug+Hyp mice ($p<0.01$ vs. Nor and $p<0.001$ vs. Hyp mice); while RV$\pm$dP/dt$_{max}$ was increased from 1712.5 ± 67.3 mmHg/s in Nor mice to 2299.5 ± 115.7 mmHg/s in Hyp mice ($p<0.001$) and 2812.6 ± 93.8 mmHg/s in Sug+Hyp mice ($p<0.001$ vs. Nor and $p<0.001$ vs. Hyp mice) (Fig. 6f and g). There was no significant difference of HR among the Nor, Hyp, and Sug+Hyp mice (453.7 ± 7.4, 438.7 ± 10.4, and 465.5 ± 3.7 bpm, respectively). The estimated or calculated mPAP was 14.7 ± 0.3 mmHg in Nor mice, 21.2 ± 0.5 mmHg in Hyp

mice ($p<0.001$ vs. Nor), and 25.8 ± 0.5 mmHg in Sug+Hyp mice ($p<0.001$ vs. Nor and $p<0.001$ vs. Hyp mice). In this study, however, we also found that the calculated RV contractile index, the ratio of RV$\pm$dP/dt$_{max}$ to RVSP, was slightly, but significantly, decreased in Hyp mice (73.0 ± 2.9 s^{-1}; $p<0.05$) and Sug+Hyp mice (72.3 ± 2.3 s^{-1}; $p<0.05$) in comparison to Nor mice (82.0 ± 1.7 s^{-1}) (Fig. 6g).

Using HPH mice, we also conducted a prevention experiment to test the effect of 2-aminoethyl diphenylborinate (2-APB), a non-selective blocker of cation channels. The

---

Box 2 Protocol for measuring PA wall thickness using histological approach and H&E staining.

1. Anesthetize mouse by injecting pentobarbital (i.p., 120 mg/kg) and appropriate anesthesia was verified by checking for lack of tactile response when pinching footpads.
2. Restrain mouse on surgical pad under microscope with ventral side facing up.
3. Make a midline vertical cervical skin incision and expose the ventral side of trachea by dissecting the midline raphe which separates fatty tissue on the left and right sides.
4. Once the trachea was clearly seen, hooks were inserted on both sides of the skin incision to open the wound and enhance visualization of the trachea.
5. Insert a cannula into the trachea through a small cut with the bent tip tilted toward the ventral surface of the mouse. Make sure that the cannula is placed below the vocal cords but well above the carina. Suture should be used to stabilize the cannula inside the trachea.
6. Slowly inject 1× PBS (5–10 ml) into the RV using a 22-G needle to superfuse the lungs. After perfusion, the lungs frequently turned to white.
7. Inject 3-ml 10% formalin (using a syringe) via the tracheal cannula to inflate the lungs. When lungs were fully inflated, the cannula was gently removed from the trachea and suture was used to tie up the trachea securely to prevent the formalin release.
8. Dissect the lungs out of the body and place the lungs in formalin for 24 h (at 1:10 ratio) to fix the lungs. The fixed lung tissues were dehydrated, embedded into paraffin, and then sectioned.
9. Process the lung tissue slice for hematoxylin and eosin (H&E) staining and generate tissue slides.
10. Deparaffinize sections twice in xylene and dehydrate sections with alcohol at a series of concentrations (twice in 100%, once in 95% and 70% alcohol).
11. Stain sections with hematoxylin and counterstain in eosin. Dehydrate sections once in 95% and twice in 100% alcohol.
12. Clear sections twice in xylene, mount slides with xylene-based mounting medium, and dry slides overnight in the hood.
13. Take images on the stained samples or lung tissue slides by an Eclipse Ti2 inverted microscope (Nikon, Japan) and process the lung tissue images using an NIS-Elements software (version 5.21.00).
14. Carefully highlight the total area of the whole PA (A_T, including intraluminal area) and the area of the PA wall (A_{PA}) using the tool menu in Photoshop software (v. 13.1.2) (see Fig. X).
15. Measure and record the highlighted whole PA area (A_T) and the highlighted PA wall area (A_{PA}) by ImageJ Analysis menu.
16. Calculate the PA wall thickness as the ratio of the area of PA wall to the area of whole PA, that is, PA wall thickness = A_{PA}/A_T, where $A_T = A_{PA}$ + intraluminal area (A_{IA}).
17. Measure and record the outer diameter (OD) of each PA section highlighted and used to calculate PA wall thickness.
18. Categorize the recorded PAs, based on OD, into three groups: (*a*) large PA (OD > 100 μm), (*b*) medium-sized PA (OD = 50–100 μm), and (*c*) small PA (OD < 50 μm).

---

prevention experimental protocol is shown in Fig. 7a, along with the chemical structure of 2-APB (Fig. 7b) and its blockade effect on cation influx through receptor-operated cation channels (Fig. 7c), in which 2-APB was intraperitoneally injected to mice once a day starting from the beginning of hypoxic exposure to the end. Four weeks later, RHC was performed on all three groups of mice (Fig. 7a) to measure and compare hemodynamics (Fig. 7d and e) and angiography parameters (Fig. 7f and g) in normoxic control mice, chronically hypoxic mice injected with vehicle and chronically hypoxic mice injected with 2-APB (1 mg/kg, i. p., q.d.). The data demonstrated that intraperitoneal injection of 2-APB at the beginning of hypoxic exposure ameliorated or inhibited the development of HPH. As shown in Fig. 7d and e, RVSP and RV ± dP/dt_{max} in Nor mice (20.4 ± 0.4 mmHg and 1672.8 ± 68.7 mmHg/s) were increased to 35.4 ± 0.5 mmHg and 2969.0 ± 253.3 mmHg/s ($p < 0.001$), respectively. In Hyp+2-APB mice, RVSP and RV ± dP/dt_{max} dropped to 29.6 ± 1.1 mmHg and 2180.8 ± 133.4 mmHg/s, respectively (Fig. 7e). These data indicate that intraperitoneal injection of 2-APB once a day resulted in 38.6 ± 7.2% (from 15.0 ± 0.5 mmHg in Hyp mice to 9.2 ± 1.1 mmHg in Hyp+2-APB mice) and 60.8 ± 10.3% (from 1296.2 ± 253.3 in Hyp mice

to 508.0 ± 133.4 mmHg in Hyp+2-APB mice) inhibition of hypoxia-induced increases in RVSP and RV ± dP/dtmax, respectively (Fig. 7e). Furthermore, 2-AP resulted in 38.6 ± 7.2% inhibition (from 9.1 ± 0.3 mmHg in Hyp mice to 5.6 ± 0.7 mmHg in Hyp+2-APB mice) of hypoxia-induced increase in mPAP. In these experiments, hypoxia increased RV ± dP/dt_{max} (mainly due to the increase in RVSP) and 2-APB significantly inhibited hypoxia-induced increase in RV ± dP/dt_{max}. Neither hypoxia nor 2-APB affected RV contractile index and heart rate (Fig. 7e). These data indicate that intraperitoneal injection of the non-selective cation channel blocker, 2-APB, partially prevented or significantly inhibited mice from developing hypoxia-induced PH.

The increased RVSP (and mPAP) in chronic hypoxic mice was associated with significantly decreased the lung angiography parameters, while 2-APB partially preserved the total length of branches, the number of branches, and the number of junctions measured in the middle peripheral areas (Fig. 7f and g). Four weeks of hypoxic exposure decreased the total length of lung vascular branches from 22.2 ± 0.6 mm/mm^2 in Nor mice to 13.9 ± 0.9 mm/mm^2 in Hyp mice ($p < 0.001$); while 2-APB resulted in 65.4 ± 4.1% restoration of hypoxia-induced decrease
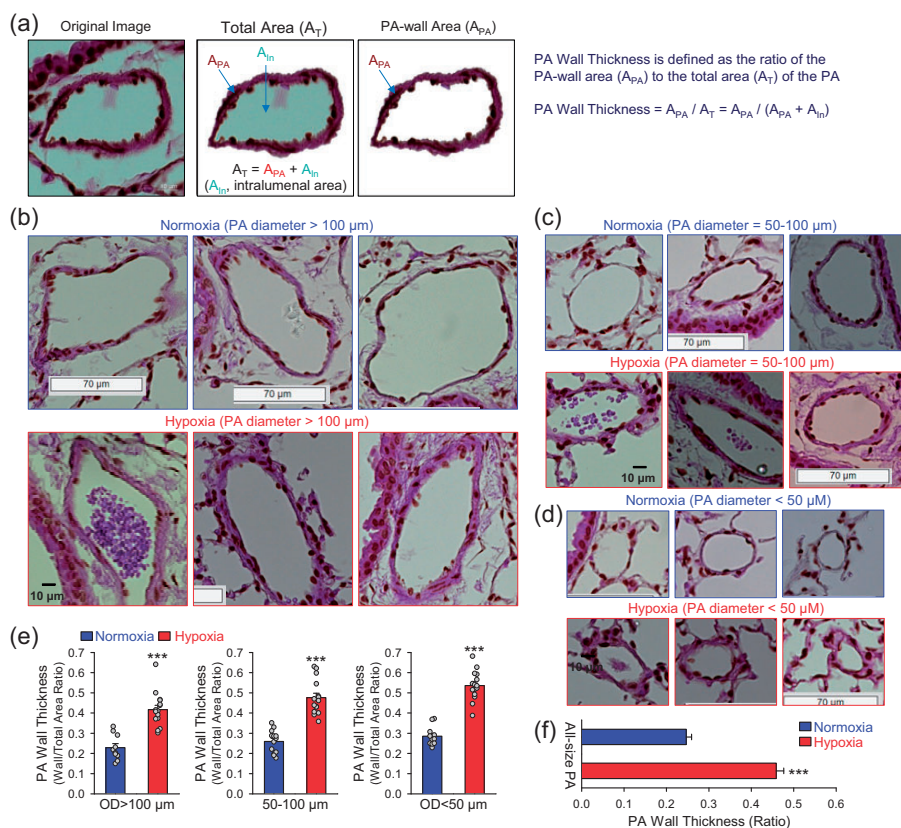
Fig. 5. Pulmonary vascular remodeling or arterial wall thickening in mice with experimental pulmonary hypertension. (a) Example images of mouse pulmonary artery (PA) stained with hematoxylin and eosin (H&E) showing the steps of morphometric analysis of PA wall thickness. Different areas in the original image (left panel) were highlighted to measure PA-wall area (A_{PA}) (middle panel) and total area (A_T) (right panel). The PA wall thickness was calculated as a ratio of A_{PA} to A_T (A_{PA}/A_T), while A_T is the sum of PA-wall area (A_{PA}) and intraluminal area (A_{In}) ($AT = A_{PA} + A_{In}$). (b-d) Representative H&E images of the large [outer diameter (OD) > 100 μm; b], medium-sized (50 < OD < 100 μm; c) and small (OD < 50 μm; d) pulmonary arteries (PAs) from mice exposed to normoxia or normobaric hypoxia for four weeks. (e) Summarized data showing PA wall thickness measured as the ratio of PA wall area to total PA area (A_{PA}/A_{In}) in large (n = 10 and 15), medium-sized (n = 13 and 15) and small (n = 11 and 15) PAs from normoxic and hypoxic mice. (f) Summarized data (mean±SE, n = 35 and 45) showing PA wall thickness in all size of PAs from normoxic and hypoxic mice. ***$p < 0.001$ vs. Normoxia.

(from -8.3 ± 0.9 mm/mm^2 in Hyp mice to -2.9 ± 0.3 mm/mm^2 in Hyp+2-APB mice, $p < 0.01$) (Fig. 7g). Furthermore, decreased the number of branches and the number of junctions from 548.9 ± 25.2 mm^{-2} and 290.9 ± 12.5 mm^{-2} in Nor mice to 217.3 ± 25.6 mm^{-2} ($p < 0.001$) and 103.2 ± 12.5 mm^{-2} ($p < 0.001$) in Hyp mice, respectively. 2-APB resulted in $61.5 \pm 4.1\%$ restoration of hypoxia-induced decrease of the number of branches (from -331.6 ± 25.6 mm^2 in Hyp mice to -127.8 ± 13.6 mm^{-2} in Hyp+2-APB mice, $p < 0.01$) and $57.6 \pm 4.1\%$ restoration of hypoxia-induced decrease of the number of junctions (from -187.8 ± 12.5 mm^{-2} in Hyp mice to -79.6 ± 7.7 mm^{-2} in Hyp+2-APB mice, $p < 0.001$) (Fig. 7g). These observations imply that 2-APB-mediated partial prevention or significant inhibition of HPH in mice is due, at least in part, to 2-APB-mediated regression of pulmonary vascular remodeling.

RV hypertrophy

Increased pulmonary vascular resistance due to sustained pulmonary vasoconstriction and concentric pulmonary vascular remodeling in animals with experimental PH increases afterload burden for the RV and results in RV hypertrophy. A simple method to measure RV hypertrophy, which also confirms increased afterload or increased pulmonary arterial pressure in mice with experimental PH, is to measure the ratio of the weight of isolated RV wall to the weight of remaining left ventricle (LV) and septum (S). The increase of RV/(LV+S) ratio, referred to as Fulton Index (Ref), is used to indicate the RV hypertrophy. The weight of the RV or the Fulton Index was measured or calculated by the protocol shown in the Box 4 and in Fig. 8a.

When the whole heart including right and left ventricles and atria as well as the main PA and aorta was isolated or
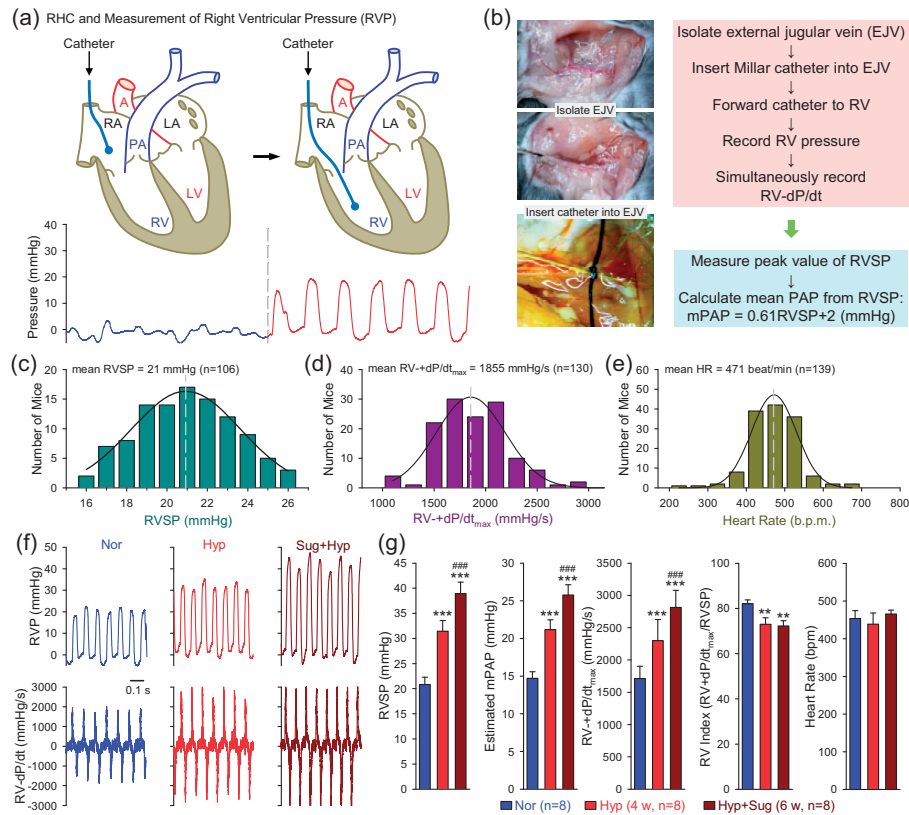
Fig. 6. Right heart catheterization in mice to measure pulmonary hemodynamics. (a) A diagram showing the position of catheter in the right atria (RA) and right ventricle (RV) (upper panels) as well as the respective record of RA pressure (blue) and RV pressure (red) (lower panel). (b) Images of external jugular vein (EJV) and simplified protocol to measure RV pressure (RVP) and RV contractility (RV ± dP/dt). The mean pulmonary artery pressure (mPAP) is calculated from RV systolic pressure (RVSP) using the following equation: mPAP = 0.61 × RVSP + 2 (mmHg). (c–e) Histograms showing the distribution of the values of RVSP (c, n = 106), RV ± dP/dt$_{max}$ (d, n = 130), and heart rate (HR, e, n = 139) in normal mice. Mean RVSP (21 mmHg), RV ± dP/dt$_{max}$ (1855 mmHg/s) and HR (471) shown in the graphs are the maximal or peak values of the fitted curves, as indicated by vertical broken lines. (f) Representative records of RV pressure (RVP, upper panels) and RV contractility (RV ± dP/dt, lower panels) in normoxic (Nor), chronically hypoxic (Hyp, for four weeks) and sugen/hypoxia (Sug+Hyp, for six weeks) mice. (g) Summarized data (mean ± SE, n = 8) showing RVSP, estimated mPAP, RV ± dP/dt$_{max}$, calculated RV contractile index (the ratio of RV ± dP/dt$_{max}$ to RVSP), and HR in Nor, Hyp and Sug+Hyp mice. **$p < 0.01$, ***$p < 0.001$ vs. Nor; ###$p < 0.001$ vs. Hyp (one-way ANOVA).

Box 3 Protocol for measuring RVSP and RV±dP/dt via RHC in mice.

1. Place the catheter in warm PBS for at least 30 min to achieve stable recordings.
2. Set up the Millar catheter system including the catheter transducer and the data acquisition system.
3. Initiate anesthesia by weighing the mouse gently and placing in a chamber containing isoflurane at a concentration of 2.5%. Maintain anesthesia by restraining the sedated mouse on a heating pad, taping the upper and lower limbs at a isoflurane concentration of between 1 and 1.5%.
4. Restrain the sedated mouse on a styrofoam board with autoclave tape and place the mouse under a dissecting microscope (8× magnification).
5. Make an incision of skin at the right side of the neck, remove surrounding connective and fat tissues, and carefully dissect and expose the right external jugular vein.
6. Place two sutures below the vein, one lose suture near to the chest and one tight suture away from chest.
7. Cut a tiny hole (one third of the diameter of the vein) into the exposed right external jugular vein using fine micro scissors under microscope and gently insert the catheter into the hole of the isolated vein and tie the knot just tight enough.
8. Advance the catheter into the right ventricle by constantly monitoring the pressure waveform change from the venous pressure, to the right atrial pressure and eventually to the right ventricular pressure (RVP).
9. Record RVP and RV-dP/dt for 3 min when the records become stable, and save the records for analysis.
10. Analyze RVSP (right ventricular systolic pressure) and RV-dP/dt data using LabChart Pro 7.0 software and perform statistical analysis using SigmaPlot software.
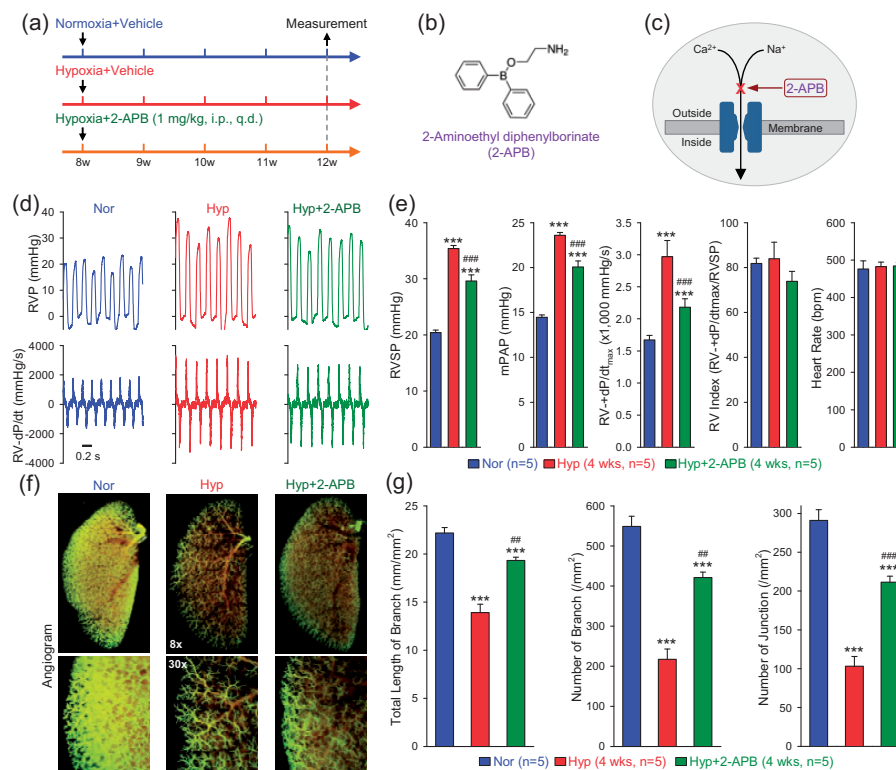11. Calculate mean PAP according to the equation: mPAP = 0.61 × RVSP + 2 (mmHg).

Fig. 7. Inhibitory effect of intraperitoneal injection of 2-APB on hypoxia-induced pulmonary hypertension (HPH) in mice. (a) Experimental protocol for the prevention experiment using 2-APB. Eight-week-old C57Bl/6 mice are subjected to normoxia (Nor, room air or 21% O_2) or hypoxia (10% O_2) for four weeks. 2-APB (1 mg/kg, q.d.) was intraperitoneally injected (i.p.) at the beginning of hypoxia exposure and continuously injected for four weeks during hypoxia. (b) Chemical structure of 2-APB. (c) Diagram showing that 2-APB blocks Ca^{2+} (or Na_+) influx through a receptor-operated cation channel. (c) Representative records of right ventricular pressure (RVP) (upper panels) and RV contractility (RV $\pm$ dP/dt) (lower panels) in normoxic (Nor) mice, hypoxic (Hyp) mice and Hyp mice receiving 2-APB (1 mg/kg, i.p., q.d., for two weeks after four weeks of hypoxia exposure). (d) Summarized data (mean $\pm$ SE, n = 5) showing RV systolic (RVSP), estimated mean pulmonary arterial pressure (mPAP), RV $\pm$ dP/dt$_{max}$, RV contractility index (RV $\pm$ dP/dt$_{max}$/RVSP) and heart rate in Nor, Hyp and Hyp+2-APB mice. ***$p < 0.001$ vs. Nor; ###$p < 0.001$ vs. Hyp (one-way ANOVA). (e) Representative angiography images of the left lung at 8$\times$ (upper panels) and 30$\times$ (lower panels) magnification from Nor, Hyp, and Hyp+2-APB mice. (f) Summarized data (mean $\pm$ SE, n = 5) showing the total length of lung vascular branches(left panel), the number of lung vascular branches (middle panel) and the number of lung vascular branch junctions (right panel) per square millimeter of the selected peripheral lung area from Nor, Hyp, and Hyp+2-APB mice. ***$p < 0.001$ vs. Nor; ##$p < 0.01$, ###$p < 0.001$ vs. Hyp (one-way ANOVA).

Box 4 Protocol for measuring Fulton Index in mice.

1. Euthanize the mouse immediately by intraperitoneal injection of pentobarbital sodium (120 mg/kg) after right heart catheterization.
2. Isolate the whole heart including aorta and main PA from the mouse and place it onto absorbent paper like Kimwipes delicate task wiper to get rid of blood.
3. Carefully remove the main PA, aorta and right and left atria from the heart without damaging the ventricles.
4. Open the right ventricle (RV) and carefully isolate the RV by dissecting it out along the interventricle septum.
5. Weigh the RV and the remaining heart (i.e., the left ventricle and the septum) to record the weight of the RV and the weight of left ventricle (LV) and septum (S).
6. Calculate the Fulton Index, the ratio of the weight of RV to the weight of LV and S [RV/(LV+S)]; increased which is used to indicate RV hypertrophy.

dissected out from the mouse, make sure to get rid of the blood inside and surround the heart using absorbent paper or surgical gauze pads. Among 77 hearts isolated from normal wildtype mice, our study indicated that the Fulton Index ranged from 0.2 to 0.3, with an averaged Fulton Index of 0.229 ± 0.043 (Fig. 8b). In chronically hypoxic mice, the Fulton Index increased to 0.3736 ± 0.0104 (n = 33) (Fig. 8c); the 77.7% increase of Fulton Index from normoxic control mice (0.2202 ± 0.0053, n = 50) to chronically hypoxic mice (0.3736 ± 0.0104 (n = 33) is
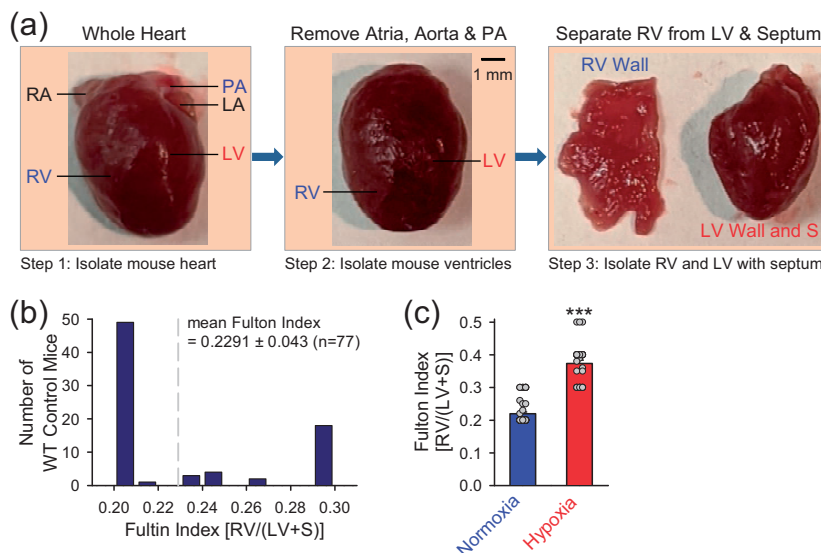
Fig. 8. Fulton index is increased in chronically hypoxic mice. (a) Experimental diagram depicting the isolated whole heart (left), the ventricles without the main PA, aorta and atria (middle), and the isolated RV (right). (b) Histogram of Fulton index, the ratio of the weight of RV to the weight of the left ventricle (LV) and septum (S) [RV/(LV+S)]. (c) Summarized data (means±SE) showing Fulton Index [RV/(LV+S)] (left panel) in normoxic control mice (Normoxia, n = 50) and chronically hypoxic mice (Hypoxia, n = 30). ***$p < 0.001$ vs. Normoxia.

associated with 44.8% increase in mPAP (Fig. 7d and e), 84.1% increase in PA wall thickness (Fig. 5f) and 37.3%–64.5% decreases in the total length of lung vascular branches and the numbers of branches and junctions determined by ex vivo angiogram (Fig. 7g). These data indicate that pulmonary hemodynamics (e.g., RVSP, mPAP) measured by RHC, lung vascular wall thickness measured by histology and H&E staining, lung vascular density and branches determined by ex vivo angiogram, and Fulton Index estimated by the ratio of RV weight to LV+S weight are reliable measurements to estimate phenotype changes occurs in mice with experimental PH.

Discussion

Despite advances in our understanding of the pathogenic mechanisms and pathophysiology of PAH and PH, current therapies are limited to slowing disease progression and relieving symptoms. Many important cellular signaling pathways and potential therapeutic targets in PAH/PH have been discovered using *in vitro* model systems, but the clinical utility of these studies rely on validation *in vivo*. Therefore, animal models provide an important link between discoveries at the bench-top and new treatments at the patient bedside.

A good small animal (or mouse) model of PH that recapitulates the common pathophysiological and pathological features shown in patients with PH is needed for studying pathogenic mechanisms and testing new drug effects on inhibition or regression of PH. In this study, we sought to describe a commonly used set of experimental approaches we have used for ex vivo and in vivo studies on pathogenic

mechanisms and therapeutic interventions of PH using the mouse model of mild and severe PH. A good mouse model of PH and a standard set of experimental readouts can be used to test the pathogenic role and therapeutic potential of specific genes involved in the development and progression of the disease. Phenotypical characterization in mice with experimental PH is also a prerequisite for linking the disease or pathogenic features to specific genes in global, conditional, and/or inducible knock-out and transgenic mice. Advancement in genomic and molecular technology has enabled us to do more in-depth studies on genetic and epigenetic mechanisms involved in the disease initiation and progression. The phenotypical characterization on, for example, pulmonary hemodynamics, RV function, arterial pressure, and vascular remodeling in animal models of the disease is critical for defining the pathogenic mechanisms and developing novel therapies for PAH/PH.

In this study, we described a hands-on experimental approach to measure pulmonary hemodynamics in vivo by RHC, determine lung vascular density (or remodeling) ex vivo by angiography, and quantify lung vascular wall thickness ex vivo by histology.

Our lung angiogram data showed that the total length of vascular branches, the number of branches and the number of junctions in the selected peripheral areas of the mouse lung at the apical, middle, and basal areas were comparable in normal mice. The total length of branches, the number of branches, and the number of junctions in a given area (mm^{-2}) in the peripheral area were comparable between female and male mice. Furthermore, we found that a short-time (4–6 min) RHC procedure did not alter the measured lung vascular density by angiogram; that is, the total

length of branches, the number of branches and the number of junctions in a given area (mm^{-2}) in the peripheral area of the lung were comparable between control mice and mice underwent RHC.

In our lung histology and H&E staining experiments, we defined PA wall thickness as the ratio of the PA wall area (A_{PA}) to the total PA cross-section area (i.e., A_{PA} and intraluminal area, A_{in}). Our data indicated that chronically hypoxic mice exhibited significantly thickened large ($OD > 100\,\mu m$), middle-sized ($OD = 50–100\,\mu m$) and small ($OD < 50\,\mu m$) PAs, or increased PA wall thickness calculated by the ratio of $A_{PA}/(A_{PA}+A_{in})$. The outer diameter (OD) of PA in the cross-section images was estimated by averaging the length of straight diameter lines (usually 4–8 lines) between the PA wall and across the center of the PA.

In our hemodynamic measurement via RHC, we found that RVSP in normal mice ranges from 16 to 26 mmHg with an averaged value at 21 mmHg. In addition to directly measuring RVSP and RV contractility ($RV \pm dP/dt$), we also estimated mean PAP based on the equation: $mPAP = 0.61$ RVSP $+0.2$ (in mmHg) and calculated RV contractile index based on the equation: RV contractile index $= RV \pm dP/dt_{max}/RVSP$ (in s^{-1}). Four-week exposure to normobaric hypoxia (10% O_2) in a hypoxic chamber resulted in an increase in RVSP by approximately 10 mmHg and an increase in mPAP by 6.5 mmHg, while injection of sugen5416 (once a week for four weeks), a vascular endothelial growth factor (VEGF) receptor blocker, increased RVSP by 18 mmHg and mPAP by 11 mmHg, respectively. The 10–18 mmHg increases in RVSP in mice with HPH and 6.5–11 mmHg increases in mPAP in mice with SuHx-PH provided a good range of hemodynamic change in the mouse models of PH for in vivo pharmacological experiments. Indeed, intraperitoneal injection of 2-APB (1 mg/kg, q.d. for four weeks) resulted in a 6-mmHg decrease in RVSP (or 38% inhibition of the hypoxia-induced increase in RVSP) and a 5.7 mmHg decrease in mPAP (or 38% inhibition of the hypoxia-induced increase in mPAP) in mice with HPH. The inhibitory effect of 2-APB on HPH seemed to be at least partially due to its inhibitory effect on pulmonary vascular remodeling as indicated by lung angiogram.

Pulmonary vascular remodeling, featured by concentric pulmonary wall thickening and obliterative intimal lesions, is one of the major causes for the elevated PVR in patients with PAH and other forms of pre-capillary PH. Intraluminal narrowing and partial or complete occlusion of small arteries due to pulmonary vasoconstriction and vascular remodeling would all limit the perfusion and distribution of the contrast, Microfil® polymer mixture, and decrease measures of the total length of lung vascular branches, the number of vascular branches, and the number of branch junctions, as shown in angiogram data. Therefore, the decreased total length of branches and the numbers of branches and junctions observed by the

angiography experiments do not necessarily indicate that the vascular branches are physically lost. The decreases of the measured parameters indicate pulmonary arterial intraluminal narrowing, peripheral arterial occlusion, arteriole and precapillary muscularization, and pulmonary vasoconstriction that limit or restrict perfusion and distribution of the contrast, Microfil® polymer mixture, into the pulmonary vasculature, especially the peripheral small arterial branches.

The angiogram data in this study are also consistent with the histological data showing significant vascular wall thickening of different sizes of pulmonary arteries in mice with HPH. The ability to observe the entire pulmonary vascular tree via angiogram can provide a more general demonstration of distal pulmonary arterial remodeling compared to lung histological images (H&E staining). To further characterize the pulmonary vascular remodeling revealed by angiography and histological approach, we recommend doing immunohistochemistry experiment to further characterize the cell proliferation markers (e.g., PCNA5, Ki67 for increased cell proliferation) and the mesenchymal cell markers (e.g., SMA, vimentin for muscularization, and fibrosis). Furthermore, the mouse model of PH can also be used to determine lineal tracing[38] and examine whether conditional and inducible knockout or knockdown of specific genes can exert therapeutical or reversal effect on established PH.[7,9,10,39]

In summary, this study provides a simple and reliable set of combined experimental approaches using lung angiogram, RHC, and lung histology to characterize, phenotypically, pathophysiological and pathological changes in mice with experimental PH. The experimental protocol and mouse models can be used for drug development and pre-clinical drug screening, defining pathogenic mechanisms of pulmonary vascular remodeling (using knock-out, knock-in, and transgenic mice) and genetically associated investigation (e.g., mutant knock-in and CRISPR/Cas9 gene-editing).[39] Although no animal models can exactly recapitulate all pathophysiological and pathological features of human PAH, the mouse model of PH and the detailed experimental protocols provide a useful and reliable experimental strategy to study pulmonary vascular disease. We recommend that in vitro experiments using tissue/cell specimens from patients with PAH as well as ex vivo and in vivo animal experiments be used in parallel to study pathogenic mechanisms and developing therapeutic interventions for pulmonary vascular disease.

Author contributions

ORCID iDs

Jifeng Li https://orcid.org/0000-0002-0418-6151
Ayako Makino https://orcid.org/0000-0003-1259-8604
Jason X.-J. Yuan https://orcid.org/0000-0002-0685-4862

References

1. Simonneau G, Montani D, Celermajer DS, et al. Haemodynamic definitions and updated clinical classification of pulmonary hypertension. *Eur Respir J* 2019; 53: 1801913.
2. Mandegar M, Fung YC, Huang W, et al. Cellular and molecular mechanisms of pulmonary vascular remodeling: role in the development of pulmonary hypertension. *Microvasc Res* 2004; 68: 75–103.
3. Morrell NW, Adnot S, Archer SL, et al. Cellular and molecular basis of pulmonary arterial hypertension. *J Am Coll Cardiol* 2009; 54: S20–S31.
4. Hemnes AR, Beck GJ, Newman JH, et al. PVDOMICS: a multi-center study to improve understanding of pulmonary vascular disease through phenomics. *Circ Res* 2017; 121: 1136–1139.
5. Hassoun PM, Mouthon L, Barbera JA, et al. Inflammation, growth factors, and pulmonary vascular remodeling. *J Am Coll Cardiol* 2009; 54: S10–S19.
6. Schermuly RT, Ghofrani HA, Wilkins MR, et al. Mechanisms of disease: pulmonary arterial hypertension. *Nature Rev Cardiol* 2011; 8: 443–455.
7. Smith KA, Voiriot G, Tang H, et al. Notch activation of Ca^{2+} signaling in the development of hypoxic pulmonary vasoconstriction and pulmonary hypertension. *Am J Resp Cell Mol Biol* 2015; 53: 355–367.
8. Yoo HY, Zeifman A, Ko EA, et al. Optimization of isolated perfused/ventilated mouse lung to study hypoxic pulmonary vasoconstriction. *Pulm Circ* 2013; 3: 396–405.
9. Tang H, Babicheva A, McDermott KM, et al. Endothelial HIF-2a contributes to severe pulmonary hypertension due to endothelial-to-mesenchymal transition. *Am J Physiol* 2018; 314: L256–L275.
10. Tang H, Chen J, Fraidenburg DR, et al. Deficiency of Akt1, but not Akt2, attenuates the development of pulmonary hypertension. *Am J Physiol* 2015; 308: L208–L220.
11. Tam AYY, Horwell AL, Trinder SL, et al. Selective deletion of connective tissue growth factor attenuates experimentally-induced pulmonary fibrosis and pulmonary arterial hypertension. *Int J Biochem Cell Biol* 2021; 134: 105961.
12. Weissmann N, Dietrich A, Fuchs B, et al. Classical transient receptor potential channel 6 (TRPC6) is essential for hypoxic pulmonary vasoconstriction and alveolar gas exchange. *Proc Natl Acad Sci U S A* 2006; 103: 19093–19098.
13. Stenmark KR, Meyrick B, Galie N, et al. Animal models of pulmonary arterial hypertension: the hope for etiological discovery and pharmacological cure. *Am J Physiol* 2009; 297: L1013–L1032.
14. Stenmark KR, Fagan KA and Frid MG. Hypoxia-induced pulmonary vascular remodeling: cellular and molecular mechanisms. *Circ Res* 2006; 99: 675–691.
15. Dempsey EC, Wick MJ, Karoor V, et al. Neprilysin null mice develop exaggerated pulmonary vascular remodeling in response to chronic hypoxia. *Am J Pathol* 2009; 174: 782–796.
16. Steiner MK, Syrkina OL, Kolliputi N, et al. Interleukin-6 overexpression induces pulmonary hypertension. *Circ Res* 2009; 104: 236–244, 228p following 244.
17. Frank DB, Lowery J, Anderson L, et al. Increased susceptibility to hypoxic pulmonary hypertension in Bmpr2 mutant mice is associated with endothelial dysfunction in the pulmonary vasculature. *Am J Physiol* 2008; 294: L98–L109.
18. Bauer NR, Moore TM and McMurtry IF. Rodent models of PAH: are we there yet? *Am J Physiol* 2007; 293: L580–L582.
19. Heath D. The rat is a poor animal model for the study of human pulmonary hypertension. *Cardioscience* 1992; 3: 1–6.
20. Voelkel NF and Tuder RM. Hypoxia-induced pulmonary vascular remodeling: a model for what human disease? *J Clin Invest* 2000; 106: 733–738.
21. Zaiman A, Fijalkowska I, Hassoun PM, et al. One hundred years of research in the pathogenesis of pulmonary hypertension. *Am J Resp Cell Mol Biol* 2005; 33: 425–431.
22. Taraseviciene-Stewart L, Kasahara Y, Alger L, et al. Inhibition of the VEGF receptor 2 combined with chronic hypoxia causes cell death-dependent pulmonary endothelial cell proliferation and severe pulmonary hypertension. *FASEB J* 2001; 15: 427–438.
23. Ciuclan L, Bonneau O, Hussey M, et al. A novel murine model of severe pulmonary arterial hypertension. *Am J Resp Crit Care Med* 2011; 184: 1171–1182.
24. Kojonazarov B, Hadzic S, Ghofrani HA, et al. Severe emphysema in the SU5416/hypoxia rat model of pulmonary hypertension. *Am J Respir Crit Care Med* 2019; 200: 515–518.
25. Bogaard HJ, Legchenko E, Ackermann M, et al. The adult Sprague-Dawley Sugen-Hypoxia rat is still "the one:" a model of Group 1 pulmonary hypertension: reply to Le Cras and Abman. *Am J Respir Crit Care Med* 2020; 201: 621–624.
26. Poble PB, Phan C, Quatremare T, et al. Therapeutic effect of pirfenidone in the Sugen/hypoxia rat model of severe pulmonary hypertension. *FASEB J* 2019; 33: 3670–3679.
27. Bootman MD, Collins TJ, Mackenzie L, et al. 2-aminoethoxydiphenyl borate (2-APB) is a reliable blocker of store-

operated Ca^{2+} entry but an inconsistent inhibitor of InsP$_3$-induced Ca^{2+} release. *FASEB J* 2002; 16: 1145–1150.

28. Chen GL, Zeng B, Eastmond S, et al. Pharmacological comparison of novel synthetic fenamate analogues with econazole and 2-APB on the inhibition of TRPM2 channels. *Br J Pharmacol* 2012; 167: 1232–1243.

29. Hendron E, Wang X, Zhou Y, et al. Potent functional uncoupling between STIM1 and Orai1 by dimeric 2-aminodiphenyl borinate analogs. *Cell Calcium* 2014; 56: 482–492.

30. Lemonnier L, Prevarskaya N, Mazurier J, et al. 2-APB inhibits volume-regulated anion channels independently from intracellular calcium signaling modulation. *FEBS Lett* 2004; 556: 121–126.

31. Rae MG, Hilton J and Sharkey J. Putative TRP channel antagonists, SKF 96365, flufenamic acid and 2-APB, are non-competitive antagonists at recombinant human a1b2g2 GABA(A) receptors. *Neurochem Int* 2012; 60: 543–554.

32. Xi Q, Adebiyi A, Zhao G, et al. IP$_3$ constricts cerebral arteries via IP$_3$ receptor-mediated TRPC3 channel activation and independently of sarcoplasmic reticulum Ca^{2+} release. *Circ Res* 2008; 102: 1118–1126.

33. Chemla D, Castelain V, Humbert M, et al. New formula for predicting mean pulmonary artery pressure using systolic pulmonary artery pressure. *Chest* 2004; 126: 1313–1317.

34. Parasuraman S, Walker S, Loudon BL, et al. Assessment of pulmonary artery pressure by echocardiography – a comprehensive review. *Int J Cardiol Heart Vasc* 2016; 12: 45–51.

35. Ma W, Han W, Greer PA, et al. Calpain mediates pulmonary vascular remodeling in rodent models of pulmonary hypertension, and its inhibition attenuates pathologic features of disease. *J Clin Invest* 2011; 121: 4548–4566.

36. Tabima DM, Hacker TA and Chesler NC. Measuring right ventricular function in the normal and hypertensive mouse hearts using admittance-derived pressure-volume loops. *Am J Physiol Heart Circ Physiol* 2010; 299: H2069–H2075.

37. Wang Z and Chesler NC. Pulmonary vascular wall stiffness: an important contributor to the increased right ventricular afterload with pulmonary hypertension. *Pulm Circ* 2011; 1: 212–223.

38. Crnkovic S, Marsh LM, El Agha E, et al. Resident cell lineages are preserved in pulmonary vascular remodeling. *J Pathol* 2018; 244: 485–498.

39. West JD, Chen X, Ping L, et al. Adverse effects of BMPR2 suppression in macrophages in animal models of pulmonary hypertension. *Pulm Circ* 2019: 2045894019856483.